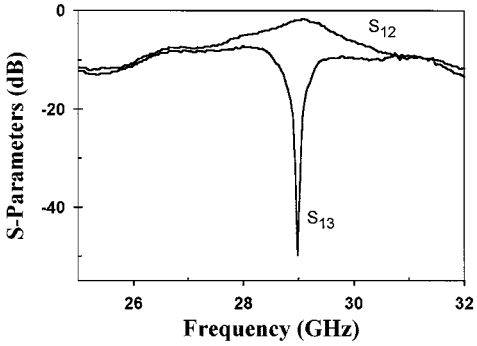

Fig. 4. Normalized scattering parameter (S_{21}, S_{31}) results versus frequency for the same circulator as shown in Fig. 3, with this circulator biased with $H < 1.5$ kOe.

circulator circuit bandwidth, nor did it prove possible to adjust the frequency where maximum isolation occurs to coincide with the minimum in S_{11}. However, these improvements further indicate the importance of the hexaferrite magnetic properties, and the state of magnetization, in determining the circulator performance.

Considerable improvements can be expected in the performance of the circulator circuits presented here by developing hexaferrite materials having large coercive fields and smaller magnetic and dielectric absorption, and by improved tuning and decreased losses in the microstrip matching network. In addition, transmission-line losses might be greatly reduced at the systems level by designing other components to match the low-output impedance of these thin planar circulators. With these refinements, integrated planar hexaferrite circulators may become as prevalent as ferrite waveguide components.

REFERENCES

[1] E. F. Schloemann, "Circulators for microwave and millimeter-wave integrated circuits," *Proc. IEEE*, vol. 76, pp. 188–200, Feb. 1988.

[2] J. D. Adam, H. Buhay, M. R. Daniel, M. C. Driver, G. W. Eldridge, M. H. Hanes, and R. L. Messham, "Monolithic integration of an X-band circulator with GaAs MMIC's," in *IEEE MTT-S Int. Microwave Symp. Dig.*, 1995, pp. 97–99.

[3] S. A. Oliver, P. M. Zavracky, N. E. McGruer, and R. Schmidt, "A monolithic single-crystal yttrium iron garnet/silicon X-band circulator," *IEEE Microwave Guided Wave Lett.*, vol. 7, pp. 239–241, Aug. 1997.

[4] H. How, S. A. Oliver, S. W. McKnight, P. M. Zavracky, N. E. McGruer, C. Vittoria, and R. Schmidt, "Theory and experiment of thin-film junction circulator," *IEEE Trans. Microwave Theory Tech.*, vol. 46, pp. 1645–1653, Nov. 1998.

[5] N. Zeina, H. How, C. Vittoria, and R. West, "Self-biasing circulators operating at Ka-band utilizing M-type hexagonal ferrites," *IEEE Trans. Magn.*, vol. 28, pp. 3219–3221, Sept. 1992.

[6] J. A. Weiss, N. G. Watson, and G. F. Dionne, "New uniaxial-ferrite millimeter-wave junction circulators," in *IEEE MTT-S Int. Microwave Symp. Dig.*, vol. 1, 1989, pp. 145–148.

[7] Y. Akaiwa and T. Okazaki, "An application of a hexagonal ferrite to a millimeter-wave Y circulator," *IEEE Trans. Magn.*, vol. MAG-10, pp. 374–378, June 1974.

[8] M. A. Tsankov and L. G. Milenova, "Design of self-biased hexaferrite waveguide circulators," *J. Appl. Phys.*, vol. 73, pp. 7018–7020, May 1993.

[9] P. Campbell, *Permanent Magnet Materials and Their Application*. Cambridge, U.K.: Cambridge Univ. Press, 1994.

[10] J. J. Green and F. Sandy, "Microwave characterization of partially magnetized ferrites," *IEEE Trans. Microwave Theory Tech.*, vol. MTT-22, pp. 641–645, June 1974.

Accurate RF Large-Signal Model of LDMOSFETs Including Self-Heating Effect

Youngoo Yang, Jaehyok Yi, and Bumman Kim

***Abstract*—In this paper, we present a new silicon RF LDMOSFET large-signal model including a self-heating effect. A new empirical channel current model suited for accurately predicting intermodulation distortion is employed. The proposed channel current model can represent transconductance (gm) saturation and rolloff in the continuous manner. It has continuous higher order derivatives for accurate prediction of nonlinear microwave circuit behavior, such as power amplifiers, microwave mixers, oscillators, etc. Using the complete large-signal model, we have designed and implemented a 1.2-GHz power amplifier. The measured and simulated amplifier characteristics, especially the intermodulation and harmonic behaviors, are in good agreement.**

***Index Terms*—Empirical channel current model, large-signal model, LDMOS, self-heating effect.**

I. INTRODUCTION

The recent advances of the silicon RF LDMOSFET technology make it possible to use the device for over 2-GHz band [1]. Due to the high gain and good linearity, LDMOSFET offers a good alternative to GaAs MESFET and silicon bipolar junction transistor (BJT) for L- or S-band power amplifiers [1]. For the circuit design using a nonlinear circuit simulator, an accurate large-signal model in the RF band is required. Previous physical models, such as the BSIM3V3, have too many parameters and too complex extraction routines [2], [3]. The table-based models have problems with a relatively long simulation time, no capability to include self-heating effects, and less accuracy to predict distortion behavior of power amplifiers [2]–[4]. Miller *et al.* [5] introduced an empirical large-signal model of RF LDMOSFET. However, Miller's model could not express the channel current saturation for a large gate-bias voltage. This may cause an inaccurate rolloff of transconductance. Here, we propose a compact channel current model with improved characteristics. It employs fewer parameters, but accurately describes transconductance rolloff to near zero and self-heating effect.

For power amplifiers, self-heating could lead to the premature breakdown of the device, and could degrade the power performance to a considerable extent with a large rise in channel temperature [6], [7]. In LDMOSFET, like conventional MOS transistors, the self-heating degrades the effective mobility and linearly reduces the threshold voltage (V_T). Thus, the temperature rise increases the drain current due to the reduced threshold voltage at a low-current region and decreases it due to the effective mobility degradation at a high-current region [8], [9]. Hence, a large-signal model must describe the self-heating effect properly.

In this paper, we present an accurate LDMOSFET large-signal model including a dynamic self-heating effect. A new channel current model equation has a continuous expression of transconductance (gm) and its higher order derivatives ($gm2$, $gm3$, ...) to accurately predict intermodulation distortion characteristics of the nonlinear microwave circuits. It includes thermal circuit of a low-pass structure to account

Manuscript received August 18, 1999.

The authors are with the Department of Electronics and Electrical Engineering, Microwave Application Research Center, Pohang University of Science and Technology, Pohang, Kyungbuk 790-784, Korea.

Publisher Item Identifier S 0018-9480(01)01083-3.

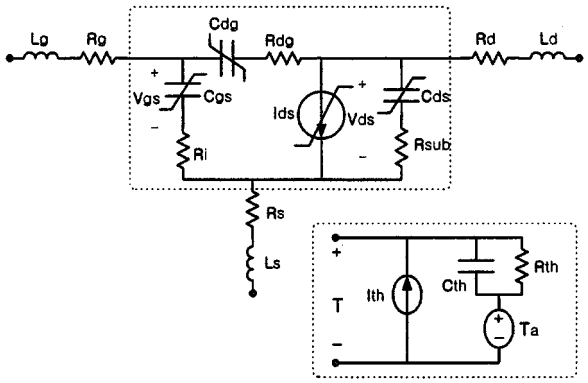

Fig. 1. Large-signal equivalent circuit of an RF LDMOSFET with a thermal circuit.

for self-heating effect. To verify modeling results, an 1.2-GHz power amplifier is designed using harmonic-balance simulation and implemented. The measured and simulated results are presented.

II. Large-Signal Model

The large-signal model of an RF LDMOSFET is made up of several lumped passive linear components, nonlinear capacitances, nonlinear current source, and additional thermal circuits, as shown in Fig. 1 [2], [3], [10]–[12].

In a large-signal model, the gate–source and drain–source voltage-dependent channel current model is the most important element because it is the major nonlinear component [13]. We measure I–V using a pulsed technique with different ambient temperatures to obtain the temperature-dependent channel current parameters.

The proposed channel current model is formulated as follows:

$$I_{\rm ds} = I_{gm} \cdot \tanh\Big[\alpha(T) \cdot V_{\rm ds}\Big] \cdot \Big[1 + \lambda(T) \cdot V_{\rm ds}\Big] \tag{1}$$

where $\alpha(T)$ is the current saturation parameter and $\lambda(T)$ is the channel length modulation parameter. $T\,^\circ$C is the channel temperature. The channel current model of (1) is a very simple form, representing all operation regions by a single equation. I_{gm} represents the channel current versus gate voltage

$$I_{gm} = \beta(T) \cdot \left\{ V_{gm} + \ln\Big[\exp(V_{gm}) + \exp(-V_{gm})\Big] \right\} \tag{2a}$$

$$V_{gm} = A \cdot \left(1 - \frac{1}{{V_{gm1}}^{VGMEXP}}\right) - C \tag{2b}$$

$$V_{gm1} = \epsilon + \frac{1}{2} \cdot \left\{ \tanh\Big[\zeta \cdot (1 + Vgs - V_T)\Big] + 1 \right\} \cdot \Big|1 + Vgs - V_T\Big| \tag{2c}$$

$$V_T = V_{T0}(T) + V_{T1} \cdot V_{\rm ds} \tag{2d}$$

where $\beta(T)$ is the temperature-dependent transconductance coefficient, V_T is the threshold voltage, and V_{gm}, which is a function of V_{gm1}, A, and C, can be interpreted as the surface potential that determines the inversion charge. V_{gm} converges to A–C for a large $V_{\rm gs}$. This V_{gm} allows a realistic depletion, inversion, strong inversion, and saturation region transitions. As V_{gm} increases from subthreshold, I_{gm} increases from depletion region current to inversion region current. Equation (2a) accurately describes the saturation and rolloff mechanism of transconductance. A, C, and $VGMEXP$ are fitting parameters. ϵ and ζ are very small and large constants of $1.0E-6$ and $1.0E6$, respectively.

TABLE I
Channel Current Model Parameters Including Temperature Parameters of MRF9382T1

Parameter	Value
β_0	0.79208
α_0	2.6343
λ_0	5.9888E-3
β_T	5.737E-3
α_T	-4.8889E-3
λ_T	1.1852 E-4
V_{T00}	2.43974
V_{T0T}	-1.1315E-3
V_{T1}	-1.212E-2
A	4.3477
C	0.3645
$VGMEXP$	0.7002
R_{th}	8.0 $[^\circ C/Watt]$

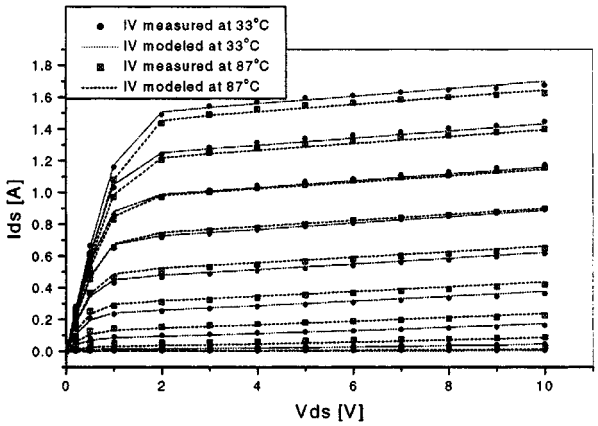

Fig. 2. Measured and modeled pulsed I–V curves at different ambient temperatures: $V_{\rm gs} = 1.8$ to 3.4 V, step $= 0.2$ V.

From (1) and (2a)–(2d), the parameters having channel temperature dependency can be written as

$$\beta(T) = \beta_0 + \beta_T \cdot T \tag{3a}$$

$$\alpha(T) = \alpha_0 + \alpha_T \cdot T \tag{3b}$$

$$\lambda(T) = \lambda_0 + \lambda_T \cdot T \tag{3c}$$

$$V_{T0}(T) = V_{T00} + V_{T0T} \cdot T. \tag{3d}$$

These temperature-dependent parameters are extracted from the pulsed I–V data at different ambient temperatures. These parameters are extracted at each temperature. From the data, temperature-dependent terms are extracted.

Thermal circuit of the RF LDMOSFET is shown at Fig. 1. It is a low-pass circuit with shunting $R_{\rm th}$ and $C_{\rm th}$. The $R_{\rm th}$ is to represent static characteristics. Both $R_{\rm th}$ and $C_{\rm th}$ are to represent transient characteristics of the channel current to the temperature variation. From the thermal circuit of Fig. 1, the static channel temperature is given by

$$T = R_{\rm th} \cdot I_{\rm th} + T_a \tag{4a}$$

$$I_{\rm th} = I_{\rm ds} \cdot V_{\rm ds} \tag{4b}$$

where $R_{\rm th}$ $^\circ$C/W is thermal resistance, $I_{\rm th}$ W is thermal current of channel power dissipation, and T_a $^\circ$C is ambient temperature.

Table I shows the channel current parameters including the temperature parameters. The device modeled is Motorola's MRF9382T1. Fig. 2 shows the measured and modeled pulsed I–V curves at two different

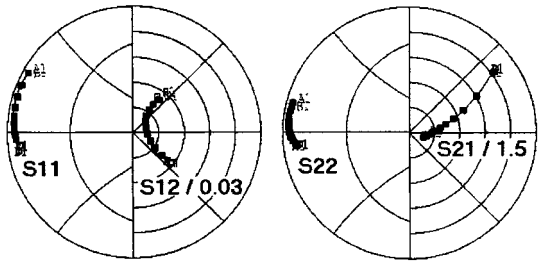

Fig. 3. Measured and modeled s-parameters: $V_{\rm gs} = 2.4$ V, $V_{\rm ds} = 6.0$ V, and frequency $= 1.0$–3.3 GHz.

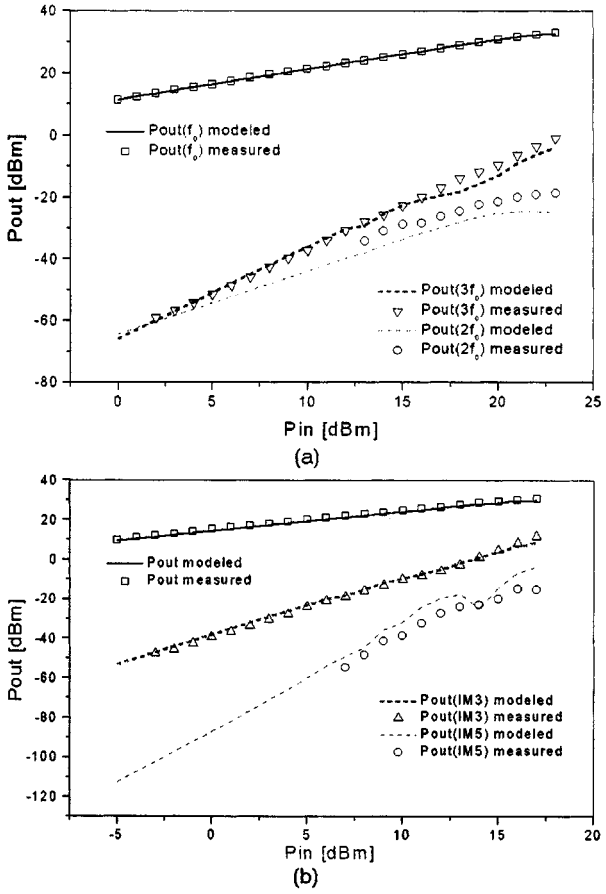

Fig. 4. Simulated and measured amplifier characteristics: $V_{\rm ds} = 6.0$ V, $I_{\rm ds} = 274$ mA. (a) When single-tone input is applied. (b) When two-tone input is applied.

temperatures of 33 °C and 87 °C. It can be shown that the new channel current model accurately describes channel current with channel temperature variations.

III. Experimental Verification of the Model

This large-signal model has been implemented at HP's MDS using symbolic defined device (SDD). Measured and modeled I–V characteristics have been already shown at Fig. 2. The small-signal s-parameters are compared at Fig. 3. S-parameters, which have a frequency range of 1.0–3.3 GHz, are measured at room temperature of 33 °C and at $V_{\rm gs} = 2.4$ V, $V_{\rm ds} = 6.0$ V of quiescent bias point. As shown in this figure, the measured and modeled parameters are fitting very well.

For verification of the large-signal model, a single-stage class-AB power amplifier at 1.2 GHz is designed using MDS. This amplifier has short termination circuits for the second-order harmonics at both source and load using $\lambda/4$ bias lines. Thus, the second-order harmonic power is fully reflected back to the device. We have built a hybrid-type power amplifier with a simple open-stub matching network. In the source matching, a series 3-Ω resistor is connected to enhance the stability of the power amplifier. Input and output matching conditions are $Z_S = 7.3 + j1.49$ and $Z_L = 2.15 - j0.47$. A power test is performed for both one- and two-tone cases.

At $V_{\rm ds} = 6.0$ V and $I_{\rm ds} = 274$ mA of quiescent point, this amplifier has 1-dB gain compression output power of 33.0 dBm and $\rm IMD_3$ of 27.83 dBc at an average output power of 29.0 dBm under class-AB operation. The power gain is 11.3 dB. Single-tone measurement results are shown in Fig. 4(a). When a 1.2-GHz single-tone input is applied, the measured and simulated output power and the third-order harmonic power are in good agreement. The measured second-order harmonic power is well matched to the trend of simulated data, nevertheless the imperfection of harmonic short termination. Fig. 4(b) shows the two-tone measurement results of the power amplifier. The tones are separated by 0.5 MHz and the center frequency is 1.2 GHz. The simulated and measured two-tone average output power, $\rm IM_3$ (third-order intermodulation) power, and $\rm IM_5$ (fifth-order intermodulation) power versus input power show reasonably good agreement.

IV. Conclusion

A new large-signal model suited for silicon RF LDMOSFET has been developed. The proposed channel current model has continuous higher order derivatives and the capability of expressing transconductance rolloff in a continuous manner to accurately simulate nonlinear microwave circuits. It also includes a dynamic self-heating effect. The measured and simulated small-signal s-parameters and pulsed I–V data are in good agreement. To verify the new large-signal model, the second-order harmonic terminated power amplifier was designed and implemented. This model predicts the fundamental and harmonic power very well, indicating that our model is well suited for the nonlinear RF circuit design.

References

[1] W. Alen, W. Brakensiek, C. Dragon, and W. Burger, "120–W 2-GHz Si LDMOS RF power transistor for PCS base station applications," in *IEEE MTT-S Int. Microwave Symp. Dig.*, 1998, pp. 707–710.

[2] W. R. Curtice, J. A. Pla, D. Briges, T. Lian, and E. E. Shumate, "A new electro-thermal nonlinear model for silicon RF LDMOS FETs," in *IEEE MTT-S Int. Microwave Symp. Dig.*, 1999, pp. 419–422.

[3] L. Bengtsson, I. Angelov, H. Zirath, and J. Olsson, "An empirical high-frequency large-signal model for high-voltage LDMOS transistors," in *Proc. EuMC*, vol. 1, 1998, pp. 733–735.

[4] J. M. Collants, J. J. Raoux, R. Quere, and A. Suarez, "New measurement-based technique for RF LDMOS nonlinear modeling," *IEEE Microwave Guided Wave Lett.*, vol. 8, pp. 345–347, Oct. 1998.

[5] M. Miller, T. Dinh, and E. Shumate, "A new empirical large signal model for silicon RF LDMOSFET," in *IEEE MTT-S Int. Microwave Symp. Dig.*, Vancouver, BC, Canada, 1997, pp. 19–22.

[6] P. Perugupalli, M. Trivedi, K. Shenai, and S. K. Leong, "Modeling and characterization of an 80-V silicon LDMOSFET for emerging RFIC applications," *IEEE Trans. Electron Devices*, vol. 45, pp. 1468–1478, July 1998.

[7] F. F. Oettinger, D. L. Blackburn, and S. Rubin, "Thermal characterization of power transistors," *IEEE Trans. Electron Devices*, vol. ED-23, pp. 831–838, Aug. 1976.

[8] Y. P. Tsividis, *Operation and Modeling of the MOS Transistor*. New York: McGraw-Hill, 1987.

[9] M.-C. Hu and S.-L. Jang, "An analytical fully-depleted SOI MOSFET model considering the effects of self-heating and source/drain resistance," *IEEE Trans. Electron Devices*, vol. 45, pp. 797–801, Apr. 1998.

[10] M. Chan, K. Y. Hui, C. Hu, and P. K. Ko, "A robust and physical BSIM3 nonquasi-static transient and AC small-signal model for circuit simulation," *IEEE Trans. Electron Devices*, vol. 45, pp. 834–841, Apr. 1998.

[11] R. Sung, P. Bendix, and M. B. Das, "Extraction of high-frequency equivalent circuit parameters of submicron gate-length MOSFET's," *IEEE Trans. Electron Devices*, vol. 45, pp. 1769–1775, Aug. 1998.
[12] J.-P. Raskin, R. Gillon, J. Chen, D. Vanhoenacker-Janvier, and J.-P. Colinge, "Accurate SOI MOSFET characterization at microwave frequencies for device performance optimization and analog modeling," *IEEE Trans. Electron Devices*, vol. 45, pp. 1017–1025, May 1998.
[13] T. M. Roh, Y. Kim, Y. Suh, W. Sang Park, and B. Kim, "A simple and accurate MESFET channel-current model including bias-dependent dispersion and thermal phenomena," *IEEE Trans. Microwave Theory Tech.*, vol. 45, pp. 1252–1255, Aug. 1997.

A Low-Cost Uniplanar Sampling Down-Converter with Internal Local Oscillator, Pulse Generator, and IF Amplifier

Jeong S. Lee and Cam Nguyen

***Abstract*—In this paper, we report on the development of a new integrated-circuit sampling down-converter having its own pulse generator, local oscillator (LO), and IF amplifier. The internal pulse generator uses a step recovery diode together with a unique ultra-wide-band hybrid junction to generate sub-nanosecond balanced pulses for gating the sampling diodes. The down-converter exhibits a conversion gain from 12 to 15.5 dB over an RF frequency of 0.01–3 GHz with 10-MHz LO and sampling pulses of about 100 ps. Return loss at the RF port is better than 15 dB over this RF bandwidth. The down-converter exhibits a good linearity and low harmonic levels. This down-converter employs a coplanar waveguide and slot line to make the entire circuit uniplanar and is, thus, suitable for low-cost production. In addition, it has an internal pulse generator, LO, and IF amplifier, making it a compact receiver subsystem, which can readily be used in many microwave systems.**

***Index Terms*—MIC, mixer, receiver, sampler, uniplanar circuit.**

I. Introduction

A sampling down-converter is an important component in many systems such as sampling oscilloscopes, microwave counters, phase-locked instruments, and radar [1]–[5]. In particular, compact and low-cost sampling down-converters are very desirable. Existing sampling down-converters use a combination of planar and uniplanar transmission lines, requiring two-sided circuit processing, which results in high complexity and fabrication cost. Completely uniplanar sampling down-converters, in which all of the circuit elements are located on one side of the substrate, are highly desired for simplicity and low cost. These unique advantages are attained because uniplanar structures allow ease in mounting solid-state devices, elimination of via holes, and only one-sided circuit processing.

In this paper, we describe a new integrated-circuit sampling down-converter using sequential or coherent sampling. This sampling scheme, having a relatively low sampling rate, is generally used in pulsed surface penetrating radar. This down-converter has its own local oscillator (LO), pulse generator, and IF amplifier, making it a complete receiver subsystem. It is completely fabricated using a (uniplanar) coplanar waveguide (CPW) and slot line. In addition, novel configurations for the sampling head and pulse generator are used to achieve less-distortion sampling pulses and high conversion gain by exploiting the combined advantages of a CPW and slot line. The sampling head of the down-converter uses a two-diode sampling bridge to make a balanced structure for good inter-port isolations and cancellation of AM noise from the LO. The pulse generator employs a step recovery diode (SRD) and an ultra-wide-band hybrid junction to create two opposite pulses for gating (or turning on/off) the sampling diodes. In the first design, we achieve a conversion gain of 12–15.5 dB over 0.01–3-GHz RF bandwidth with 10-MHz LO and 100-ps sampling pulses. More than 15-dB RF return loss has also been measured. The down-converter has good linearity and harmonic rejection.

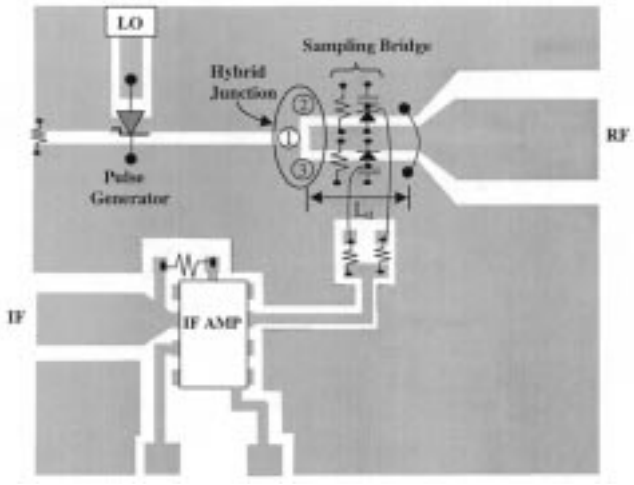

Fig. 1. Layout of the sampling down-converter.

II. Circuit Design

Fig. 1 shows the layout of the sampling down-converter, consisting of a sub-nanosecond pulse generator, hybrid junction, sampling head, LO, and IF amplifier. The main components are the pulse generator, hybrid junction, and sampling head. The pulse generator generates a step function from the LO signal, which is then fed to the hybrid junction to produce two opposite pulses for gating the sampling diodes. The sampling head is used to sample, hold, and convert the RF signal into an IF signal. They are described in details as follows.

A. Sub-Nanosecond Pulse Generator and Hybrid Junction

Pulse generators have been developed using microstrip lines and SRDs [2], [4]. SRDs are perhaps the most commonly used devices for pulse generation. Its theory is given in details in [6]. Nonlinear transmission line implemented using a CPW and an SRD has also been used to generate a sharp-edge pulse [7]. Our sub-nanosecond pulse generator also uses an SRD, but we combine a CPW and a slot line to achieve circuit simplicity, less distortion, and ready interface with the LO and sampling head of the down- converter. These uniplanar structures also permit simple connection for the SRD.

A 10-MHz square-wave LO signal is fed to the SRD, via a 50-Ω CPW, to generate a step function. This step function divides into two

Manuscript received August 24, 1999. This work was supported in part by the Texas Department of Transportation, in part under the Texas A&M University Interdisciplinary Research Program, and in part by the Southwest Region University Transportation Center.

J. S. Lee was with the Department of Electrical Engineering, Texas A&M University, College Station, TX 77843-3128 USA. He is now with Filtronic Solid State, Santa Clara, CA 95054 USA.
C. Nguyen is with the Department of Electrical Engineering, Texas A&M University, College Station, TX 77843-3128 USA.

Publisher Item Identifier S 0018-9480(01)01084-5.